Analysis and numerical evaluation of H_∞ and H_2 optimal design schemes for an electromagnetic shunt damper

Wai Kei Ao
Doctor
Vibration Engineering Section
College of Engineering, Mathematics and Physical Sciences
University of Exeter
Exeter, United Kingdom
Email: wka203@exeter.ac.uk

Paul Reynolds*

Professor
University of Exeter
Email: p.reynolds@exeter.ac.uk

The electromagnetic coupling effect can generate electromagnetic damping to suppress disturbance, which can be utilised for vibration serviceability control in civil engineering structures. An electrodynamic actuator is used as a passive electromagnetic damper (EMD). Ideally, the EMD is assumed to be attached between the ground and the structure. The kinetic energy of the vibrating structure can be converted to electrical energy to activate the electromagnetic damping. To induce appropriate damping, the two terminals of the damper need to be closed and cascaded with a resonant shunt circuit as an electromagnetic shunt damper (EMSD). In this study, an RLC oscillating circuit is chosen. For determination of optimal circuit components and comparing against the tuned mass damper (TMD), existing H_∞ design formulae are applied. This work extends this with a detailed development of an H_2 robust optimisation technique. The dynamic properties of a footbridge structure are then selected and used to verify the EMSD optimal design numerically. The vibration suppression performance is analytically equivalent to the dynamic characteristic of the TMD and has feasible installation and better damping enhancement. To further evaluate the potential application of the EMSD, multi-vibration mode manipulation via connecting multiple RLC resonant shunt circuits is adopted. The multiple RLC shunt circuit connecting to EMD is an alternative to the single-mode control of a traditional TMD. Therefore, the EMSD can, in principle, effectively achieve suppression of single and multiple vibration modes.

*Address all correspondence related to the first author.

Nomenclature
EMD electromagnetic damper
EMSD electromagnetic shunt damper
TMD tuned mass damper

1 Introduction

Electromagnetic dampers (EMD) are a viable technology for the mitigation of vibrations in a wide range of engineered structures and therefore are extensively used in the automobile/aerospace industries and in other mechanical structures [1, 2]. These devices convert mechanical energy into electric energy by means of electromagnetic induction.

This electromagnetic coupling effect was studied by Nakamoto et al. [3] and Mizuno [4], who developed a novel EMD concept for vibration mitigation wherein the processes of generating electromagnetic force and reducing undesirable motion were verified using a coupled electromagnetic and structural finite element technique. The work presented in Fleming et al. and Behrens et al. [5–8] used electromagnetic transducers for both active and passive feedback control. Shunt electrical impedance connected to transducers to induce equivalent damping functions that mitigated the host structure's vibrations. This novel concept involved the use of controller design to tune the coil terminal voltage. A further study was then carried out by Fleming et al. [9]. This study tested a structure that featured a suspended electromagnetic coil with absorber mass that used passive and active optimal control tools to reduce host structure displacement dynamic responses. These studies demonstrate that the basic electromagnetic concept can be used as an effective vibration con-

trol technique. It has also been proposed that an electromagnetic device coupled with a shunt circuit (or control circuit) can be used to improve on overall system damping. This method of using a shunt circuit to enhance system damping can be referred to as an electromagnetic shunt damper (EMSD) [10].

These techniques have already been used in mechanical applications, particularly with respect to the control of vehicle vibrations. Kim et al. [11] studied a large scale electromagnetic configuration model in an attempt to attenuate the various undesirable motions of automobiles using an active robust control scheme. Meanwhile, Kim et al. [12] and Vander Sande et al. [13] improved vehicle vibration using electromagnetic active suspension systems and robust controller designs. These studies focused mostly on large scale prototypes used in vehicle vibration suppression. In contrast, Palomera-Arias et al. [14, 15] developed a large-scale passive electromagnetic shock absorber and used it in numerical studies to enhance the structural damping of a building. This passive linear displacement motor has been used in electromagnetic shock absorber design, and it extracts mechanical energy for use in an electrical energy device. The electromagnetic force (damping force) is therefore applied in the negative direction to alleviate disturbance. Several case studies have shown that the linear displacement motor offers the same control results as a viscous damper when the correct impendence is connected, and it can also achieve some effects that are beyond the capabilities of viscous dampers. Nakamura et al. [16] proposed a new type of rotating internal mass electromagnetic damper for seismic vibration control, which was successful in generating strong control benefits such as reducing inter-storey drift, rate of acceleration, and frequency responses at each level.

Over the last two decades, there has been increasing interest in using such electromagnetic devices for vibration control within civil engineering structures. Sodano et al. [17] used a basic EMD (eddy current damper) to enhance the damping properties of a simple, small scale, cantilever beam structure. Inoue et al. [18] demonstrated a system comprising a voice coil motor and an RC shunt circuit (EMSD) designed to increase damping. Theoretical expressions developed under optimal parameter design show that such an EMSD demonstrates behaviours similar to an equivalent tuned mass damper (TMD) [19]. Cheng and Oh [20] used a passive EMSD concept, consisting of a conductive coil and a permanent magnet at the free end of a cantilever beam with an RC series shunt circuit, to provide additional shunt damping and to mitigate vibration disturbance.

As an alternative, Niu et al. [21] utilised a RLC circuit with negative resistance by using magnet pairs and conductors. This RLC resonant shunt circuit was then applied to a cantilever beam structure to test its vibration suppression effect. After experimental testing, the proposed EMSD dynamic behaviours came close to duplicating viscous damper controlling effects; the advantages of using EMSD are the absence of Coulomb friction and the satisfactory effects of suppression vibration. This study also examined a simply supported beam under the influence of electromagnetic shunt damping vibration isolators, [22] which were used to provide vibration suppression, with shunt damping being provided by a negative impedance circuit. The use of negative impedance shunts and a negative inductance negative impedance circuit with passive EMD was proposed by Yan et al. [23]. The EMSD supplied wide broadband damping of the absorber, providing effective vibration suppression to the flexible cantilever beam. As this was a passive circuit, there was no requirement for a feedback system or real time controller design.

McDaid and Mace [24] adopted positive resistance and capacitance to connect an electromagnetic device, to provide controllable broadband shunt stiffness, and damping, to mitigate undesirable disturbances. A numerical study was carried out, [25] which proposed connecting an RLC resonant shunt circuit to an electromagnetic damper, rather than a viscous damper as commonly used in the TMD. The EMSD (voice coil motor and impedance) has also been used as a shunt damper or energy harvester [26], providing considerable shunt damping to the test structure. These studies have mainly targeted control of a single vibration mode.

The use of a piezoelectric transducer cascaded with a sequence of adaptive resonant shunt impedances and capacitances, to achieve vibration suppression of multiple modes simultaneously on a cantilever beam structure, has also been proposed [27]. The test results suggest that shunt damping could provide good damping performance with minimal phase lag. Multi-mode vibration control was also studied by Cheng and Oh [28], who used RLC circuits in series under an optimal robustness control design approach, to improve the vibration characteristics of a flexible aluminium cantilever beam. In addition, Yan et al. [29] utilised a negative RL circuit with an EMD to achieve multi-mode vibration control.

The concept of EMSD, as adopted in this paper, uses shunt circuit capacitance to provide virtual/equivalent mass, and tunes the damping properties by means of the selection of other circuit components. The H_∞ optimal design process has been proposed by previous researchers [19, 30] and this method will be utilised to derive parameters corresponding to the equivalent mass ratio, frequency ratio, and damping ratio. In this study, previous work is extended to consider an H_2 optimisation method with optimal parameters that allows minimisation of the system's total vibration energy. The theoretical dynamic response is presented to demonstrate the similarities compared with a classical TMD. After that, the robust H_∞ and H_2 optimal design formulae are applied analytically, and verified for control of single and multiple vibration modes of a laboratory test-bed footbridge structure.

This paper is structured as follows: A review of TMD H_∞ and H_2 optimisation methods for obtaining optimal tuning parameters is presented, before the second section introduces the concept of EMSD in terms of the mitigation of engineering vibrations, which is the primary motivation for this study. After that, H_∞ methodology will be outlined, and an H_2 optimisation method developed, to facilitate the optimal design of parameters for an EMSD utilising an RLC resonant circuit. The next section demonstrates one potential application of this system to a footbridge structure, with

dynamic properties determined by modal testing being used to complete EMSD design and simulation. Finally, a further extension of the H_∞ and H_2 methods is presented to facilitate control of multiple vibration modes within a structure.

2 Optimal design of a tuned mass damper

A tuned mass damper (TMD) is constructed using a mass, spring and viscous damper (dashpot). The external vibration energy acting on the main structure can be dissipated by the TMD. A typical TMD and single degree of freedom (SDOF) system is shown in Figure 1. Adding the TMD to the primary structure forms a two degree of freedom (2DOF) system; the equation of motion can be written as follows:

$$\begin{bmatrix} m_1 & 0 \\ 0 & m_2 \end{bmatrix} \begin{Bmatrix} \ddot{x}_1 \\ \ddot{x}_2 \end{Bmatrix} + \begin{bmatrix} c_1+c_2 & -c_2 \\ -c_2 & c_2 \end{bmatrix} \begin{Bmatrix} \dot{x}_1 \\ \dot{x}_2 \end{Bmatrix} + \begin{bmatrix} k_1+k_2 & -k_2 \\ -k_2 & k_2 \end{bmatrix} \begin{Bmatrix} x_1 \\ x_2 \end{Bmatrix} = \begin{Bmatrix} f \\ 0 \end{Bmatrix} \tag{1}$$

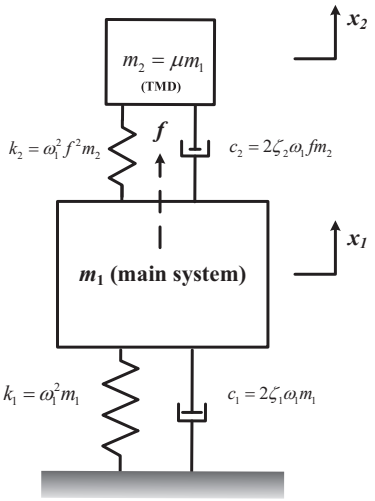

Fig. 1: TMD with single degree of freedom system under one external excitation (after [31])

In Figure 1, the SDOF primary system has dynamic properties m_1, k_1 and c_1 representing its mass, stiffness (elastic coefficient) and damping coefficient. Variable $f(t)$ is an external force acting on the primary structure. m_2, k_2 and c_2 represent the mass, stiffness and damping coefficient of the TMD. $x_1(t)$ and $x_2(t)$ represent the displacements of masses m_1 and m_2. Taking the Laplace transform of Equation 1, the transfer function between the displacement of the primary structure $X_1(s)$ and the input excitation $F(s)$ is given by:

$$\frac{X_1(s)}{F(s)} = \frac{s^2 + 2\zeta_2\omega_2 s + \omega_2^2}{\left[\begin{array}{l} m_1 s^4 + (2\zeta_2 m_2\omega_2 + c_1 + c_2)\, s^3 + \\ \left(m_1\omega_2^2 + 2\zeta_2\omega_2 c_1 + k_1 + k_2\right) s^2 + \\ \left(c_1\omega_2^2 + 2\zeta_2\omega_2 k_1\right) s + k_1\omega_2^2 \end{array}\right]} \tag{2}$$

where $\omega_2 = \sqrt{\frac{k_2}{m_2}}$ is the natural frequency and $\zeta_2 = \frac{c_2}{2\sqrt{k_2 m_2}}$ is the damping ratio of the TMD. In this theoretical development, the damping coefficient c_1 is often assumed to be zero, so that the Den Hartog method [32] can be applied to determine the optimal TMD tuning frequency and damping ratio. The assumption of zero damping in the primary structure is for minimising the response due to harmonic excitation and reduces the complexity of the mathematical derivation.

To examine the displacement frequency response function (FRF) of the primary system, it is convenient to define some ratios in advance for simplification. Mass ratio $\mu = \frac{m_2}{m_1}$ is the ratio between the mass of the TMD and that of the primary system. The frequency ratio $\gamma = \frac{\omega_2}{\omega_1}$ is the ratio between TMD frequency and the structural natural frequency. A second frequency ratio $\lambda = \frac{\omega}{\omega_1}$ is the ratio of the excitation frequency to structural natural frequency. Using these parameters, Equation 2 can be simplified and rewritten in dimensionless form, as follows:

$$H(\lambda) = \frac{X_1(\lambda)}{F(\lambda)/k_1} = \frac{\gamma^2 - \lambda^2 + j2\zeta_2\gamma\lambda}{\left[\begin{array}{l} \lambda^4 + \gamma^2 - \gamma^2\lambda^2 - \lambda^2 - \mu\gamma^2\lambda^2 + \\ j\left(-2\zeta_2\gamma\lambda^3 - 2\zeta_2\mu\gamma\lambda^3 + 2\zeta_2\gamma\lambda\right) \end{array}\right]} \tag{3}$$

2.1 TMD H_∞ optimisation

Den Hartog [32] used an optimisation procedure that disregarded the primary structure damping (i.e. $c_1 = 0$), to determine the optimal TMD tuning parameters given by frequency ratio γ_{opt} and damping ratio $\zeta_{2,opt}$ as follows:

$$\gamma_{opt} = \frac{1}{1+\mu} \tag{4}$$

$$\zeta_{2,opt} = \sqrt{\frac{3\mu}{8(1+\mu)}} \tag{5}$$

It can be seen that the optimal frequency and damping ratios are both functions of the mass ratio μ. This means that control of dynamic response is manipulated primarily by the mass ratio, which has a tuning implication, as shown in Figures 2a and 2b.

The Den Hartog method notes that the two peak values of frequency response under TMD control have equal magnitude. These two peak values are two invariant points on the

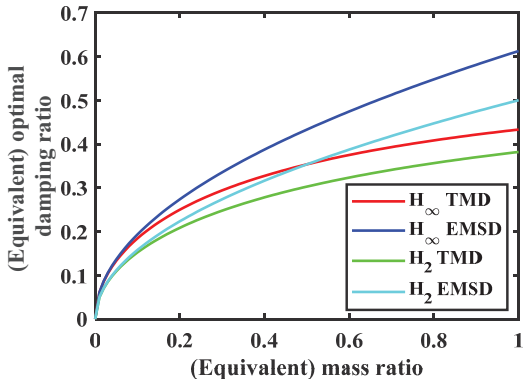

(a) Optimal damping ratio vs mass ratio

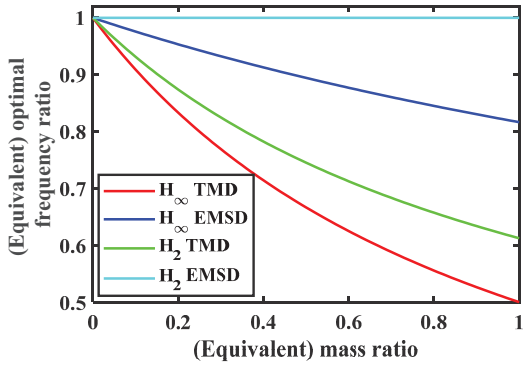

(b) Optimal frequency ratio vs mass ratio

Fig. 2: Relationship between (equivalent) mass ratio and two optimal design parameters under H_∞ and H_2 optimisation

dimensionless FRF curve. The optimal value of peak amplification factor can therefore be expressed as:

$$G_{opt} \simeq \sqrt{\frac{2+\mu}{\mu}} \tag{6}$$

Equation 6 is an approximate expression for the peak dynamic amplification factor [19].

2.2 TMD H_2 optimisation

A second optimisation method is H_2 optimisation, which aims to minimise the total vibration energy or the mean square motion of a SDOF system under random force excitations. The FRF function of a system, including a TMD, was already defined in Equation 3. Therefore, the norm of the FRF function can be written in dimensionless form, as follows:

$$|G(\lambda)| = \left|\frac{X_1(\lambda)}{F(\lambda)/k_1}\right| = \left|\frac{\gamma^2-\lambda^2+j2\zeta_2\gamma\lambda}{\left[\begin{array}{l}\left(1-\lambda^2\right)\left(\gamma^2-\lambda^2\right)-\mu\gamma^2\lambda^2+\\ j2\zeta_2\gamma\lambda\left(1-\lambda^2-\mu\lambda^2\right)\end{array}\right]}\right| \tag{7}$$

The objective of H_2 TMD optimisation is achieved by minimisation of the integral of the square of the norm of the FRF function [33], which can be expressed as:

$$\begin{aligned} &E\left[|G(\lambda)|^2\right] = \int_{-\infty}^{\infty}|G(\lambda)|^2 S_0 d\omega \\ &= \frac{\pi\omega_n S_0}{2\mu\zeta\gamma}\left[(1+\mu)^2\gamma^4+\left(4\zeta^2(1+\mu)-2-\mu\right)\gamma^2+1\right] \end{aligned} \tag{8}$$

where S_0 is the uniform power spectral density function. The exact solutions of the H_2 optimal design parameters can be derived as:

$$\gamma_{opt} = \sqrt{\frac{\mu+2}{2(\mu+1)^2}} \tag{9}$$

$$\zeta_{opt} = \frac{1}{2}\sqrt{\frac{\mu(3\mu+4)}{2(\mu+2)(\mu+1)}} \tag{10}$$

It can be observed again that the optimal frequency and damping ratios of the TMD are functions of the mass ratio. Since the H_2 optimal method considers the minimum response over the whole frequency range, equations 9 and 10 can be used to determine the values of global minimisation.

3 Electromagnetic damper with RLC resonant shunt circuit

3.1 Electromagnetic damper (EMD)

A typical concept diagram of an electromagnetic damping device is shown in Figure 3a. A permanent magnet bar and the conductive coil or material are contained within a covering shell. The conductive material is normally bonded with the shell, while the permanent magnet can move within the conductive material. The circuit diagram of the electromagnetic damper (EMD) is shown in Figure 3b, claiming that one resistor, one inductor, and a voltage source are required to represent this device graphically.

Figure 3b shows the EMD system with an open circuit, which can also be conceptualised as a circuit with infinite resistance ($I_1 = 0$, $R_{load} = \infty$). Thus, the induced current can be dissipated by the infinite resistance. Ideally, at least one circuit component must be connected to close the circuit properly, as shown in Figure 3c ($I_1 \neq 0$, $R_{load} \neq \pm\infty$).

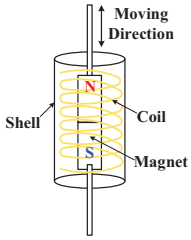

(a) EMD concept

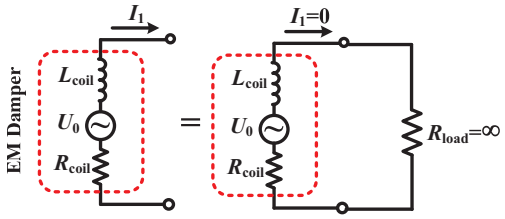

(b) Circuit expression of EMD

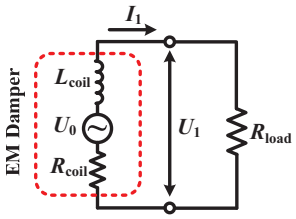

(c) EMD with closed circuit

Fig. 3: Electromagnetic damper device (after [6])

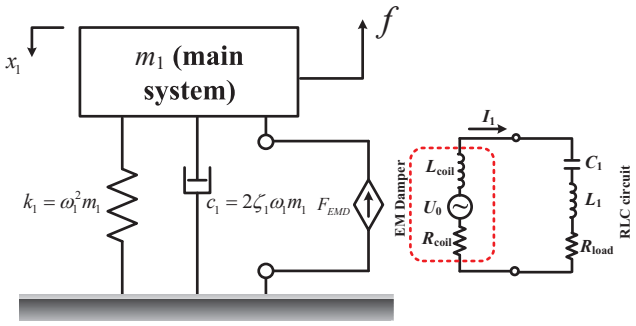

(a) SDOF structure with EMD and RLC shunt circuit

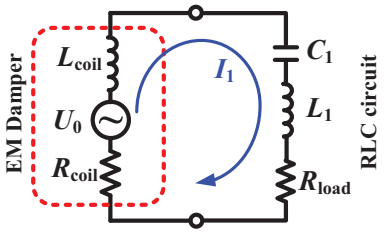

(b) Induced current (eddy current) flowing through the closed EMSD circuit

Fig. 4: Electromagnetic damper with shunt circuit

Using an EMD has several benefits. Firstly, the electromagnetic device has the capacity to dissipate energy without the need for additional mass to be added to the structure. Theoretically, there is no contact between the coil and magnets, which reduces wear and tear and friction in the device and, from a control point of view, the device can be used for both active and passive control. However, one key disadvantage is that EMD operation requires both terminal ends to be connected to the structure and to exhibit relative motion (two-port elements); this is similar to the operational requirements of a viscous damper.

3.2 EMSD H_∞ optimisation using RLC resonant shunt circuit

Figure 4a shows a SDOF system model to which an EMD has been installed in series with an RLC shunt circuit. Structural vibration (mechanical energy) generates an electromotive force (emf) in the circuit, which is proportional to the velocity of the motion, with the relationship between the two given by the machine constant K_{emV}. Multiplication of K_{emV} and velocity gives the mechanical energy that is transferred to the device, which produces the input voltage source (electrical energy) for the shunt circuit. The induced current caused by the electromagnetic coupling effect will therefore flow through the shunt circuit, as shown in Figure 4b.

When the vibration frequency is equal to the natural frequency of the RLC circuit, the reactance of the shunt circuit will be equal to zero. This implies that the circuit current will be at a maximum. It is known that damper force is proportional to the current; therefore, when the current is at a maximum, the damping force also displays its maximum value. If the RLC oscillating frequency is close to the fundamental frequency of the primary structure, the electromagnetic damper will provide a resonant-type damping effect that can suppress a single structural vibration mode extremely effectively. By combining the dynamic equation of motion in the primary system (mechanical system) and Kirchhoff's voltage law (KVL) to create a constitutive equation of the RLC shunt circuit, the whole system equation of motion can be represented as follows:

$$\begin{bmatrix} m_1 & 0 \\ 0 & L_{coil}+L_1 \end{bmatrix} \begin{Bmatrix} \ddot{x}_1 \\ \ddot{q} \end{Bmatrix} + \begin{bmatrix} c_1 & K_{emN} \\ -K_{emV} & R_{coil}+R_1 \end{bmatrix} \begin{Bmatrix} \dot{x}_1 \\ \dot{q} \end{Bmatrix} + \begin{bmatrix} k_1 & 0 \\ 0 & \frac{1}{C_1} \end{bmatrix} \begin{Bmatrix} x_1 \\ q \end{Bmatrix} = \begin{Bmatrix} f \\ 0 \end{Bmatrix} \tag{11}$$

where K_{emN} is one of the machine constants of the EMD, which gives the relationship between the electromagnetic force F_{emN} and induced current $\dot{q}$. The relationship can be written as $F_{emN} = K_{emN}\dot{q}$. Therefore, K_{emN} is used to convert the induced current into electromagnetic force. R_{coil} and L_{coil} are the resistance and inductance of the EMD. L_1, R_1 and C_1 are the total resistance, inductance and capacitance of the shunt circuit. q is an electric charge. The above equation can be rewritten in a more concise form:

$$\begin{bmatrix} m_1 & 0 \\ 0 & L \end{bmatrix} \begin{Bmatrix} \ddot{x}_1 \\ \ddot{q} \end{Bmatrix} + \begin{bmatrix} c_1 & K_{emN} \\ -K_{emV} & R \end{bmatrix} \begin{Bmatrix} \dot{x}_1 \\ \dot{q} \end{Bmatrix} + \begin{bmatrix} k_1 & 0 \\ 0 & \frac{1}{C} \end{bmatrix} \begin{Bmatrix} x_1 \\ q \end{Bmatrix} = \begin{Bmatrix} f \\ 0 \end{Bmatrix} \tag{12}$$

where R, L and C are the total resistance, inductance and capacitance of the EMSD. Taking the Laplace transform of Equation 12 with zero initial conditions gives:

$$\frac{X_1(s)}{F(s)} = \frac{Ls^2 + Rs + \frac{1}{C}}{\left[\begin{array}{l} m_1 L s^4 + (m_1 R + c_1 L)\, s^3 + \\ \left(\frac{m_1}{C} + c_1 R + k_1 L + K_{emN} K_{emV}\right) s^2 \\ + \left(\frac{c_1}{C} + R k_1\right) s + \frac{k_1}{C} \end{array}\right]} \tag{13}$$

The natural frequency and damping ratio of a simple oscillating resonant circuit (RLC) can then be defined as

$$\omega_{2,eq} = \sqrt{\frac{1}{LC}} \quad \zeta_{2,eq} = \frac{R}{2}\sqrt{\frac{C}{L}} \tag{14}$$

and therefore, Equation 13 can be rewritten as follows:

$$\frac{X_1(s)}{F(s)} = \frac{s^2 + 2\zeta_{2,eq}\omega_{2,eq}s + \omega_{2,eq}^2}{\left[\begin{array}{l} m_1 s^4 + \left(m_1 \frac{R}{L} + c_1\right) s^3 + \\ \left(m_1 \omega_{2,eq}^2 + c_1 \frac{R}{L} + k_1 + \frac{K_{emN} K_{emV}}{L}\right) s^2 + \\ \left(c_1 \omega_{2,eq}^2 + k_1 \frac{R}{L}\right) s + k_1 \omega_{2,eq}^2 \end{array}\right]} \tag{15}$$

Zhu et al. [19] compared Equations 2 and 15 and observed that the two equations have a similar form. Examining the denominator shows that the third term ($\left(m_1 \omega_{2,eq}^2 + c_1 \frac{R}{L} + k_1 + \frac{K_{emN} K_{emV}}{L}\right) s^2$) can be used to extract $\frac{K_{emN} K_{emV}}{L}$, allowing the equivalent damper stiffness to be defined as

$$k_{2,eq} = \frac{K_{emN} K_{emV}}{L} \tag{16}$$

In addition, the corresponding equivalent mass (virtual mass) and equivalent damping ratio of the EMD can be calculated using RLC circuit characteristics, as defined in Equation 14. Therefore, these can be expressed as follows:

$$m_{2,eq} = \frac{k_{2,eq}}{{\omega_{2,eq}}^2} = K_{emN} K_{emV} C \tag{17}$$

$$c_{2,eq} = 2\zeta_{2,eq}\omega_{2,eq} m_{2,eq} = \frac{K_{emV} K_{emV} RC}{L} \tag{18}$$

Substituting Equations 16, 17 and 18 into Equation 15 allows the transfer function to be presented as:

$$\frac{X_1(s)}{F(s)} = \frac{s^2 + 2\zeta_{2,eq}\omega_{2,eq}s + \omega_{2,eq}^2}{\left[\begin{array}{l} m_1 s^4 + (2m_1 \zeta_{2,eq}\omega_{2,eq} + c_1)\, s^3 + \\ \left(m_1 \omega_{2,eq}^2 + 2\zeta_{2,eq}\omega_{2,eq} c_1 + k_1 + k_{2,eq}\right) s^2 \\ + \left(c_1 \omega_{2,eq}^2 + 2k_1 \zeta_{2,eq}\omega_{2,eq}\right) s + k_1 \omega_{2,eq}^2 \end{array}\right]} \tag{19}$$

In common with conventional TMD systems, with an assumption of zero damping of the primary system, it is possible to define three ratios: $\mu_{eq} = \frac{m_{2,eq}}{m_1}$ is the ratio of equivalent mass of the EMSD to the primary structure mass, $\gamma_{eq} = \frac{\omega_{2,eq}}{\omega_1}$ is the ratio of the equivalent natural frequency of the EMSD to the natural frequency of the primary structure, and the excitation frequency ratio $\lambda = \frac{\omega}{\omega_1}$ is the same as previously described.

Therefore, the dimensionless FRF can be written as follows:

$$H_{eq}(\lambda) = \frac{X_1(\lambda)}{F(\lambda)/k_1} = \frac{\gamma_{eq}^2 - \lambda^2 + j2\zeta_{2,eq}\gamma_{eq}\lambda}{\left[\begin{array}{l} \lambda^4 + \gamma_{eq}^2 - \gamma_{eq}^2\lambda^2 - \lambda^2 - \mu_{eq}\gamma_{eq}^2\lambda^2 + \\ j\left(-2\zeta_{2,eq}\gamma_{eq}\lambda^3 + 2\zeta_{2,eq}\gamma_{eq}\lambda\right) \end{array}\right]} \tag{20}$$

To find the optimal parameters of the EMSD, the H_∞ optimisation method is used [34] and [19]. The H_∞ norm involves the minimisation of the largest singular value, and thus, the H_∞ optimisation process can be used, subject to the assumption of zero damping of the primary structure. In this study, the H_∞ optimal frequency and damping ratios of the EMSD using RLC shunt circuit can be expressed as:

$$\gamma_{opt,eq} = \sqrt{\frac{2}{2+\mu_{eq}}} \tag{21}$$

$$\zeta_{2,opt,eq} = \sqrt{\frac{3\mu_{eq}}{8}} \tag{22}$$

The equivalent frequency and damping ratios are functions of the equivalent mass ratio, as shown in Figures 2a and 2b. The equivalent mass of the EMSD (virtual mass) is a function of the capacitor. This could be used for tuning the value of the capacitor to achieve a match to the desired damper frequency, therefore reducing the peak magnitude of the system FRF. The representations of EMSD H_∞ optimal damping and frequency ratios are similar to those in a TMD. However, it is clear that one of the advantages is that there is no need to add additional mass to achieve the damping effect. Instead, the damping is achieved via selection of appropriate electrical circuit components. The design of these components is discussed later.

After the deviation of optimal frequency and damping ratios, the correlated equivalent peak dynamic amplification factor can be depicted by the equivalent mass ratio, which is given by:

$$G_{opt,eq} = |G(\lambda_a)| = \left|\frac{B}{D}\right| = \left|\frac{1}{1-{\lambda_a}^2}\right| = \left|\frac{1}{1-1\mp\sqrt{\frac{\mu_{eq}}{2+\mu_{eq}}}}\right| = \sqrt{\frac{2+\mu_{eq}}{\mu_{eq}}} \tag{23}$$

Figure 5 shows the variation of the peak amplification factor relative to equivalent mass ratio and capacitance when using an EMSD H_∞ design. It can be seen that a higher equivalent mass ratio and higher capacitance results in a lower peak amplification factor. This is analogous to a conventional TMD in that a large equivalent mass ratio produces an improved reduction in response.

3.3 EMSD H_2 optimisation using RLC resonant shunt circuit

Another robust control design approach is the H_2 optimisation method, which is used here to determine the relevant parameters of an EMSD. The H_2 optimisation method minimises the H_2 norm, by performing a minimisation of the sum of the squares of all singular values over all frequencies.

To implement the H_2 design, Cheung and Wong [33] proposed a new H_2 optimal design model of a dynamic vibration absorber which was derived by minimising the mean square motion of an SDOF system under random excitation. The results showed improved suppression of the primary structure compared with the H_∞ approach. This concept can also be applied to the optimal design of an EMSD.

The amplitude of an EMSD FRF function is expressed as:

$$|G(\lambda)| = \left|\frac{X_1(\lambda)}{F(\lambda)/k_1}\right| = \left|\frac{\gamma_{eq}^2 - \lambda^2 + j2\zeta_{2,eq}\gamma_{eq}\lambda}{\left[\begin{array}{l}\lambda^4 + \gamma_{eq}^2 - \gamma_{eq}^2\lambda^2 - \lambda^2 - \mu_{eq}\gamma_{eq}^2\lambda^2 + \\ j\left(-2\zeta_{2,eq}\gamma_{eq}\lambda^3 + 2\zeta_{2,eq}\gamma_{eq}\lambda\right)\end{array}\right]}\right| \tag{24}$$

The objective of H_2 optimisation is minimisation of the integral of the square of the amplitude of the FRF of the primary structure. It can be illustrated as

$$E\left[|G(\lambda)|^2\right] = \omega_n \int_{-\infty}^{\infty} |G(\lambda)|^2 S_0 d\lambda = \omega_n \int_{-\infty}^{\infty} \left|\frac{\gamma_{eq}^2 - \lambda^2 + j2\zeta_{2,eq}\gamma_{eq}\lambda}{\left[\begin{array}{l}\lambda^4 + \gamma_{eq}^2 - \gamma_{eq}^2\lambda^2 - \lambda^2 - \mu_{eq}\gamma_{eq}^2\lambda^2 + \\ j\left(-2\zeta_{2,eq}\gamma_{eq}\lambda^3 + 2\zeta_{2,eq}\gamma_{eq}\lambda\right)\end{array}\right]}\right|^2 S_0 d\lambda \tag{25}$$

The integration technique, from Grahshteyn and Ryzhik [35], is used to find the exact solutions of the objective function:

$$G(\lambda) = \frac{-j\lambda^3 B_3 - \lambda^2 B_2 + j\lambda B_1 + B_0}{\lambda^4 A_4 - j\lambda^3 A_3 - \lambda^2 A_2 + j\lambda A_1 + A_0} \tag{26}$$

Hence,

$$\int_{-\infty}^{\infty} |G(\lambda)|^2 d\lambda = \pi \frac{\left[\begin{array}{l}\left(\frac{{B_0}^2}{A_0}\right)(A_2A_3 - A_1A_4) + \\ A_3\left({B_1}^2 - 2B_0B_2\right) + \\ A_1\left({B_2}^2 - 2B_1B_3\right) + \\ \left(\frac{{B_3}^2}{A_4}\right)(A_1A_2 - A_0A_3)\end{array}\right]}{A_1(A_2A_3 - A_1A_4) - A_0{A_3}^2} \tag{27}$$

Using the above result, Equation 25 can be rearranged and shown as:

$$E\left[|G(\lambda)|^2\right] = \omega_n S_0 \int_{-\infty}^{\infty} \left|\frac{-\lambda^2 + j2\lambda\zeta_{2,eq}\gamma_{eq} + \gamma_{eq}^2}{\lambda^4 - j\lambda^3 2\zeta_{2,eq}\gamma_{eq} - \lambda^2\left(1 + \gamma_{eq}^2 + \mu_{eq}\gamma_{eq}^2\right) + j\lambda 2\zeta_{2,eq}\gamma_{eq} + \gamma_{eq}^2}\right|^2 d\lambda \tag{28}$$

Comparing Equations 26 and 28, the parameters can be listed as follows:

$$\begin{array}{l} A_0 = \gamma_{eq}^2 \;\; A_1 = 2\zeta_{2,eq}\gamma_{eq} \\ A_2 = 1 + \gamma_{eq}^2 + \mu_{eq}\gamma_{eq}^2 \;\; A_3 = 2\zeta_{2,eq}\gamma_{eq} \;\; A_4 = 1 \\ B_0 = \gamma_{eq}^2 \;\; B_1 = 2\,\zeta_{2,eq}\gamma_{eq} \;\; B_2 = 1 \;\; B_3 = 0 \end{array} \tag{29}$$

and thus, Equations 27, 28 and 29 can be simplified as

$$E\left[|G(\lambda)|^2\right] = \pi\omega_n S_0 \frac{\gamma_{eq}^4 + \mu_{eq}\gamma_{eq}^4 + 4\zeta_{2,eq}^2\gamma_{eq}^2 - 2\gamma_{eq}^2 + 1}{2\zeta_{2,eq}\mu_{eq}\gamma_{eq}^3} \tag{30}$$

To minimise the EMSD objective function with respect to the damping ratio, it is necessary to determine the derivative of Equation 30 and set it equal to zero:

$$E\left[|G(\lambda)|^2\right] = \frac{\pi\omega_n S_0}{2\mu_{eq}\gamma_{eq}^3}\left(\begin{array}{l}\gamma_{eq}^4\zeta_{2,eq}^{-1} + \mu_{eq}\gamma_{eq}^4\zeta_2^{-1} + \\ 4\gamma_{eq}^2\zeta_{2,eq} - 2\gamma_{eq}^2\zeta_{2,eq}^{-1} + \zeta_{2,eq}^{-1}\end{array}\right) \tag{31}$$

$$\frac{\partial}{\partial\zeta_{2,eq}} E\left[|G(\lambda)|^2\right] = \left(\begin{array}{l}-\gamma_{eq}^4\zeta_{2,eq}^{-2} - \mu_{eq}\gamma_{eq}^4\zeta_{2,eq}^{-2} + \\ 4\gamma_{eq}^2 + 2\gamma_{eq}^2\zeta_{2,eq}^{-2} - \zeta_{2,eq}^{-2}\end{array}\right) = 0 \tag{32}$$

After solving Equation 32, the optimal damping ratio can be written as

$$\zeta_{2,opt,eq} = \frac{1}{2}\sqrt{\gamma_{eq}^2 + \mu_{eq}\gamma_{eq}^2 - 2 + \frac{1}{\gamma_{eq}^2}} \tag{33}$$

To minimise the EMSD objective function with respect to the frequency ratio, a further derivative is taken:

$$E\left[|G(\lambda)|^2\right] = \frac{\pi\omega_n S_0}{2\mu_{eq}\zeta_{2,eq}}\left(\gamma_{eq} + \mu_{eq}\gamma_{eq} + 4\zeta_{2,eq}^2\gamma_{eq}^{-1} + \gamma_{eq}^{-3}\right) \tag{34}$$

$$\frac{\partial}{\partial\gamma_{eq}}E\left[|G(\lambda)|^2\right] = 1 + \mu_{eq} - 4\zeta_{2,eq}^2\gamma_{eq}^{-2} + 2\gamma_{eq}^{-2} - 3\gamma_{eq}^{-4} = 0 \tag{35}$$

Solving Equation 35, the optimal frequency ratio can be expressed as

$$\gamma_{opt,eq} = 1 \tag{36}$$

The optimal parameters of EMSD under H_2 optimisation are functions of the equivalent mass ratio, as shown in Figure 2. The equivalent frequency ratio found using the H_2 method is always close to 1 over a wide range of equivalent mass ratios. This means that the EMSD frequency and structure frequency should be equal.

Figure 6 presents a contour diagram of the EMSD H_2 optimal design, as per Equations 33 and 36. These are used to discover the value of damping of frequnecy that achieve the global minimum-the optimal design. The cross sign of Figure 6 demonstrates this minimum for relative equivalent mass ratio of 3 %. The calculation result is similar to the result for TMD H_2 optimisation.

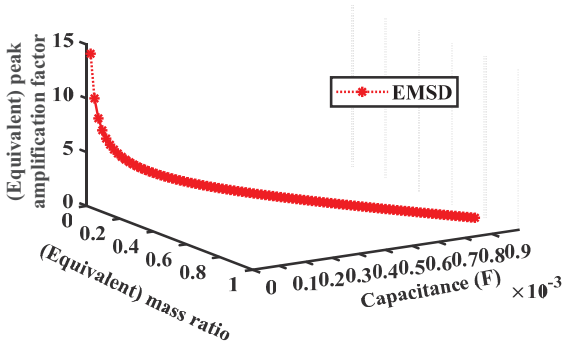

Fig. 5: EMSD H_∞ optimisation peak amplification factor and relative $\mu = 3\%$ value

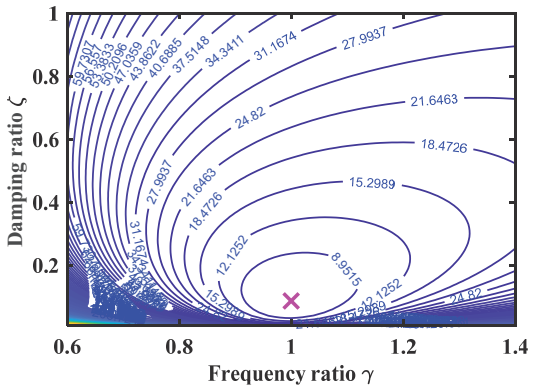

Fig. 6: Dimensionless mean square objective function of EMSD H_2 optimisation and relative $\mu = 3\%$ value

Using equations 21, 22, 33 and 36 to perform the design of the EMSD using H_∞ and H_2 optimal methods, when the values of each ratio were determined, the values of the RLC circuit components needed to be selected. The relevant calculation result is mentioned in Section 4.4. However, depending on the dynamic parameters of the structure/system being controlled, the resistors and inductors in the RLC resonant circuit might require negative values of resistance and inductance. It is noted that negative impedance/inductance circuits need to be configured with additional negative impedance/inductance converters, which could be considered a limitation of EMSD implementation. The detail of the numerical study of the negative circuit converters is discussed in other work by the authors [36].

4 Simulation of TMD and EMSD application to a footbridge structure

To carry out an analysis of the potential performance of comparative TMD and EMSD devices, the properties of a reconfigurable laboratory structure at the Vibration Engineering Section of the University of Exeter were used, as shown in Figure 7. The walking surface of the structure is formed by 12 sandwich plate system (SPS) plates of dimensions 2.49 × 1.25 m, each of which comprises two steel faceplates bonded together with a polyurethane elastomer core. The plates are subsequently supported by two main beams of size UB 457 × 191 × 82 mm, spanning 15 m. Four knife edge supports are located at the four corners of the footbridge, as shown in Figure 7.

Modal testing was carried out using shaker excitation, giving the modal properties included in Figure 8 [36].

4.1 Comparison of control using TMD and EMSD

Previous sections introduced the mathematical models for a conventional TMD and an EMD with a shunt RLC circuit (EMSD). Based on classical control theory, Figure 9 shows the difference between control systems using TMD and EMSD in the form of block diagrams.

From this point of view, the structure plant operates via TMD feedback to act as a control force to improve perfor-

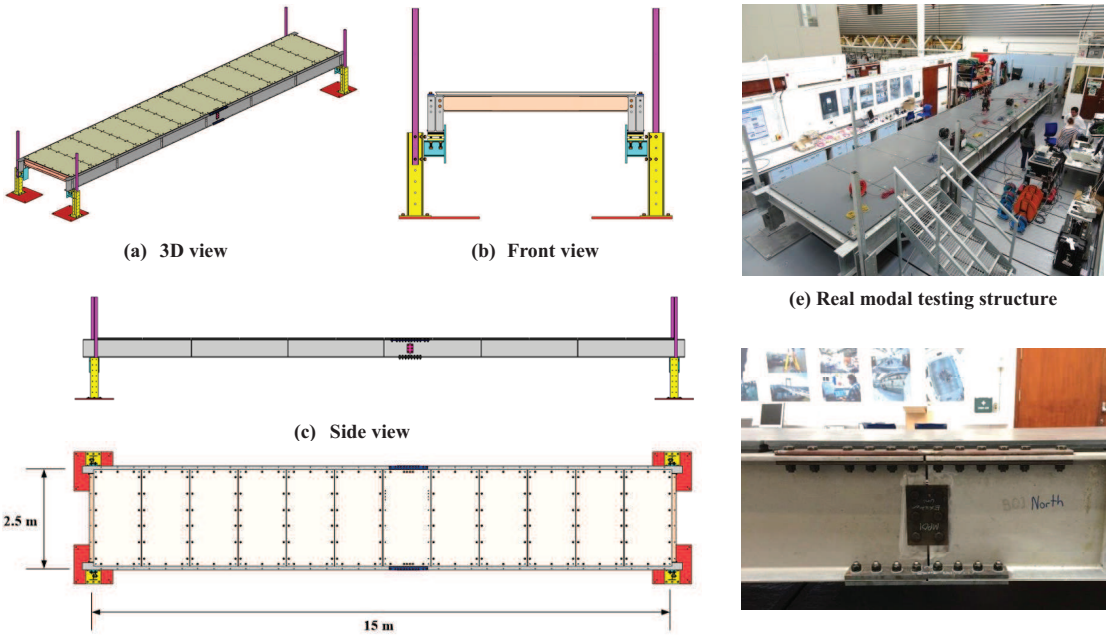

(a) 3D view (b) Front view

(c) Side view

(d) Top view

(e) Real modal testing structure

(f) Beam-beam splice moment connection with high strength friction grip (HSFG) bolts

Fig. 7: Layout of the structure

mance in passive way. The TMD requires structural vibration energy (relative motion) rather than sensor measurements. The controlling dynamics are therefore dependent on the additional mass, stiffness, and damping attached to the primary structure. As Figure 9b shows, the EMSD control concept requires the plant structure to be connected with the EMD, but this is not enough to produce a control force from the EMD. Thus, the EMD must be connected with a shunt circuit to produce the required electromotive force. Once this closed loop is complete, feedback in the form of a proper controlling force is supplied to the system plant. In this study, a passive EMSD design is used.

4.2 Specification of an electromagnetic damper

Figure 10 shows an electromagnetic actuator from APS Dynamics Inc (Model 400) that can be configured to function as an EMD. The technical characteristics of this motor are shown in Table 1. The two most important parameters are the force constant, K_{emN} and the emf constant, K_{emV}, which represent the relationships between the current and the force and between the velocity and the voltage. The previous section mentioned that the EMD can be described as an equivalent circuit component expression. Therefore, the relative inherent resistance and inductance of the EMD are 1.6 Ω and 38 mH, respectively. The two machine constants and EMD resistance and inductance can then be used for further simulation.

APS Model 400	Unit	Model 400
Effective stroke	mm	158 pk-pk
Peak force	N	445
Force constant	N/A	34.58
Back EMF	V/(m/s)	34.58
Impedance	ohm	8
Inductance	mH	53

Table 1: Technical characteristics of EMD (source: adopted from APS Dynamics Model 400 Shaker data sheet)

4.3 EMSD H_∞ and H_2 optimisation

The EMD is operated by closing the shunt circuit. From the control system block diagram in Figure 9, it is clear that the electromagnetic damper and control circuit are in series and are put in the feedback loop together. The control circuit can comprise several different circuit types but, in this study, an RLC circuit is used.

The mathematical model presented in previous section shows that the EMD with RLC circuit can be expressed as an equivalent TMD (virtual TMD). To verify that the predicted relative dynamic behaviour is similar, FRF curves can be calculated to show the separation of the primary structural mode into the two lower magnitude peaks. For this study, the mass ratio of the TMD and the equivalent mass of the EMSD are the same (3 %).

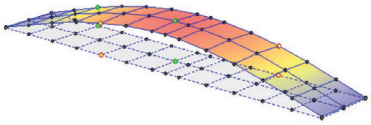

(a) 1st mode, f_1=3.8 Hz, ζ_1 = 1.01 %, m_1=6773 kg

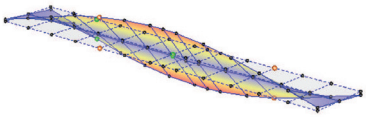

(b) 2nd mode, f_2=5.1 Hz, ζ_2 = 0.87 %, m_2=5588 kg

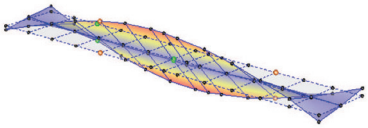

(c) 3rd mode, f_3=8.5 Hz, ζ_3 = 0.88 %, m_3=14257 kg

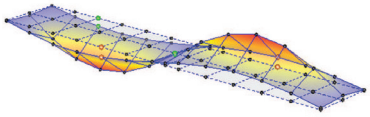

(d) 4th mode, f_4=12.4 Hz, ζ_4 = 0.78 %, m_4=1471 kg

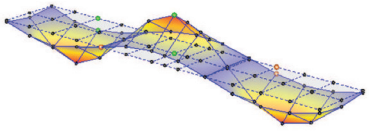

(e) 5th mode, f_5=18.6 Hz, ζ_5 = 0.51 %, m_5=2972 kg

Fig. 8: Measured mode shapes of the test structure

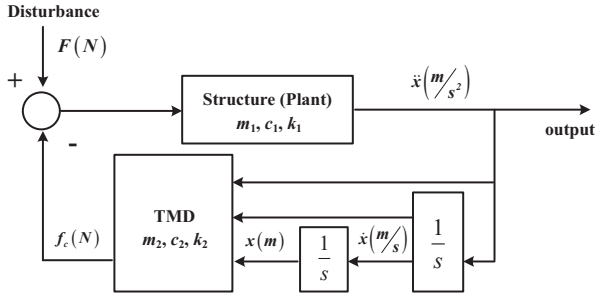

(a) Control law with passive TMD

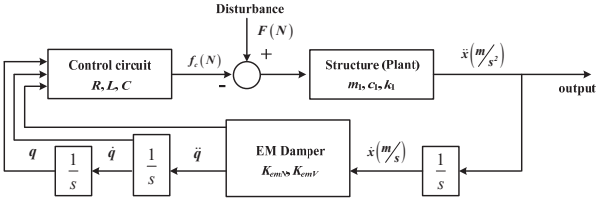

(b) Control law with EMSD

Fig. 9: Different control strategies using TMD and EMSD

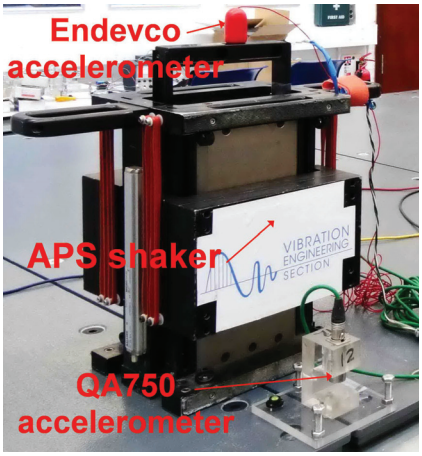

Fig. 10: Electromagnetic actuator

4.3.1 EMSD H_∞ optimisation design

The EMD has two key machine constants that determine its performance: K_{emN} and K_{emV}. Using these two parameters and the H_∞ optimisation design scheme, along with the equations given previously, a derived acceleration frequency response function (FRF) is calculated, as shown in Figures 11a (magnitude) and 11b (phase).

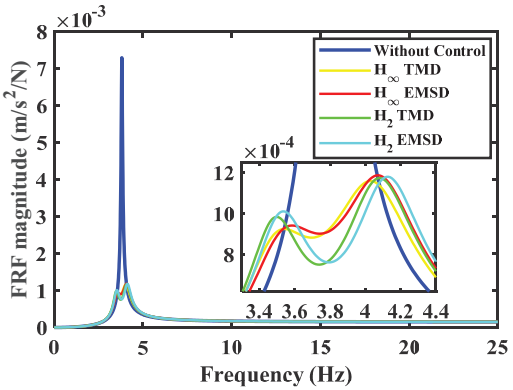

(a) Accelerance FRF magnitude

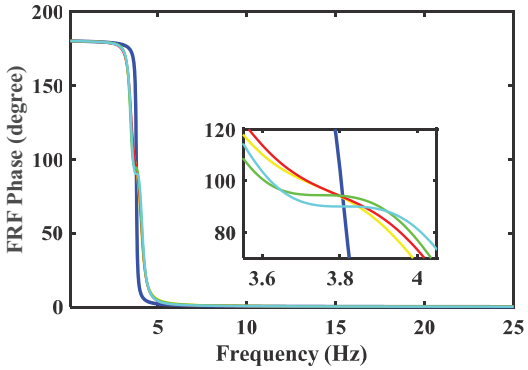

(b) Accelerance FRF phase

Fig. 11: Accelerance frequency response magnitude and phase under H_∞ and H_2 with machine constant $K_{emN} = K_{emV}$

Figure 11a shows that the EMSD FRF curve is almost the same as the equivalent TMD under H_∞ optimisation. It clearly has the typical characteristics of separation of the primary structural mode into two lower magnitude peaks. From this point of view, the equivalent TMD (or EMSD) concept can be verified. In theory, the mass ratio could be increased to more than 3 %. However, in this case, the equivalent mass ratio was limited by the electromagnetic damper's peak force.

4.3.2 EMSD H_2 optimisation design

The dynamic responses corresponding with H_2 optimisation using TMD and EMSD are also shown in Figure 11a. It should be noted that the mass ratio of this design was also set to 3 %, as in the H_∞ design. The TMD and EMSD responses are almost identical for these H_2 optimisation results under these conditions.

Further comparison shown in Figures 11a demonstrates that the H_2 FRFs have slightly lower amplitudes than H_∞ at the resonant frequency of the primary structure. For both the TMD and EMSD, the H_∞ optimisation only considers local frequency range minimisation. However, H_2 optimisation considers a wider frequency range, allowing for a better control outcome at the original structural resonant frequency.

4.4 Parametric study

Section 3 illustrates the EMSD fundamental mathematical model, which can be used to design satisfactory vibration suppression. However, in order to achieve improvements, the selected RLC circuit components must satisfy the H_∞ and H_2 optimisation design.

4.4.1 H_∞ optimisation

Equations 14, 17, 21 and 22 can be used to determine optimal resistance and inductance under H_∞ optimisation design. To obtain the relevant value of the optimal circuit components, the first step is to define the RLC circuit oscillating damping ratio by setting Equation 14 equal to the H_∞ optimal damping ratio of EMSD from Equation 22. This can be represented as follows:

$$\zeta_{2,eq} = \zeta_{2,opt,eq} \Rightarrow \frac{R}{2}\sqrt{\frac{C}{L}} = \sqrt{\frac{3\mu_{eq}}{8}} \tag{37}$$

After this, the equivalent mass ratio from Equation 17 is substituted into the above equation, so the optimal resistance is as follows:

$$R_{opt} = \sqrt{\frac{3}{2}\frac{K_{emN}K_{emV}L}{m_1}} \tag{38}$$

Using a similar concept, the general equivalent natural frequency ratio can be set to equal the optimal frequency ratio, as follows:

$$\frac{\omega_{2,eq}}{\omega_1} = \sqrt{\frac{2}{2+\mu_{eq}}} \tag{39}$$

Equations 14 and 21 can be applied to the above equation, giving:

$$L_{opt} = \frac{2m_1K_{emN}K_{emV} + m_{2,eq}K_{emN}K_{emV}}{2m_{2,eq}k_1} \tag{40}$$

It is clear that R_{opt} and L_{opt} are functions of K_{emV}, K_{emN} and $m_{2,eq}$. Equation 17 shows the equivalent mass as a function of capacitance. Equation 17 also shows that the higher the capacitance, the higher the equivalent mass. Based on the classic TMD design [32], a higher mass ratio is expected to produce a better controlling effect.

4.4.2 H_2 optimisation

The corresponding RLC circuit components under H_2 optimisation design can be derived from Equations 14, 17, 33 and 36. First, Equation 14, which outlines the RLC circuit oscillating damping ratio, should be set to equal the EMSD optimal damping ratio in Equation 33, as follows:

$$\zeta_{2,eq} = \zeta_{2,opt,eq} \Rightarrow \frac{R}{2}\sqrt{\frac{C}{L}} = \frac{1}{2}\sqrt{{\gamma_{eq}}^2 + \mu_{eq}{\gamma_{eq}}^2 - 2 + \frac{1}{{\gamma_{eq}}^2}} \tag{41}$$

After simplification, the resistance under H_2 optimal design can be obtained, as follows:

$$R_{opt} = \sqrt{\frac{\mu_{eq}L_{opt}}{C}} \tag{42}$$

Performing a similar exercise the frequency ratio uncovers the following relationship:

$$\gamma_{eq} = \gamma_{opt,eq} \Rightarrow \frac{\omega_{2,eq}}{\omega_1} = 1 \tag{43}$$

Substituting Equations 14 and 17 allow the optimal shunt circuit inductance of EMSD under H_2 optimisation method to be written as follows:

$$L_{opt} = \frac{K_{emN}K_{emV}}{m_{2,eq}\omega_1^2} \tag{44}$$

Again, when the two machine constants are fixed, the optimal resistance and inductance are functions only of capacitance. Therefore, the capacitor can act as the main parameter for tuning the optimisation design. However, Equations 42 and 44, which describe the optimal design circuit

components illustrate that, when the capacitor is set to a lower value, the resistance and inductance must take larger values to compensate. This study therefore uses a fixed value for capacitance in all component design.

To illustrate the concept, Figure 12 shows the properties of various RLC components as a function of increasing equivalent mass ratio. C, L and R are optimally determined according to Equations 17, 38, 40, 42 and 44. The triangular red marker in Figure 12a represents the selected fixed value of capacitance. The yellow circular markers in Figures 12b and 12c show the inherent EMD device inductor and resistor values, which are obtained from the EMD prototype specification data sheet in Table 1.

To compare H_∞ and H_2 optimisation designs, a specific mass ratio must be selected. In this case, the 3 % mass ratio is used. This means that the capacitance is set at 169921.07 μF, correlating with 203.19 kg of virtual mass. The optimal design results in the following parameters: total inductance of 10.42 mH under H_∞ and 10.27 mH under H_2, and total resistance of 0.053 Ω under H_∞ and 0.043 Ω under H_2. These values are indicated by the red triangular markers for H_∞ and the black triangular markers for H_2 in Figures 12b and 12c. However, these are only the targeted design values. To derive the component values of the shunt circuit, the inherent resistor and inductor (yellow markers) values of EMD must be subtracted from the results from Equations 38, 40, 42 and 44. Therefore, the RLC circuit needs to provide -42.57 mH and -7.95 Ω (green markers) for H_∞ optimisation, or -42.73 mH and -7.96 Ω (magenta markers) for H_2 optimisation.

In Figure 12b, the green and magenta markers correspond to the RLC circuit inductance values using H_∞ or H_2 optimisation designs, respectively. These inductors must provide the required negative values. In contrast, Figure 12c shows that, to meet the optimal requirements, the resistance must be a negative resistance value appropriate to either H_∞ or H_2 (green and magenta markers). The negative resistance and inductance concept are not included in this paper.

Figures 13a and 13b also illustrate how the inductance and resistance values change with variations of equivalent mass and capacitance under H_∞ and H_2 optimisation, respectively. Unsurprisingly, the inductance of the H_∞ and H_2 methods align with one another. The resistance of H_∞ and H_2 for low equivalent masses have different values. However, in the range of higher equivalent masses, they display the same values. The capacitance increases significantly for large equivalent masses, while the inductance and resistance decline dramatically as mass increases for both H_∞ or H_2 optimisation designs. This shows that inductance and resistance with capacitance have an inversely proportional relationship.

4.5 H_∞ and H_2 multi-mode control

In the previous section, single mode control via EMSD with one RLC resonant shunt circuit successfully achieved vibration suppression. The results showed that the dynamic behaviour of EMSD acted as an equivalent to TMD.

A single shunt circuit controlling single mode dynamic

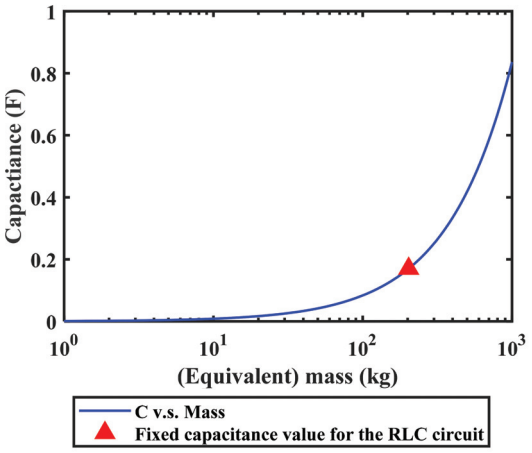

(a) Capacitance v.s. equivalent mass

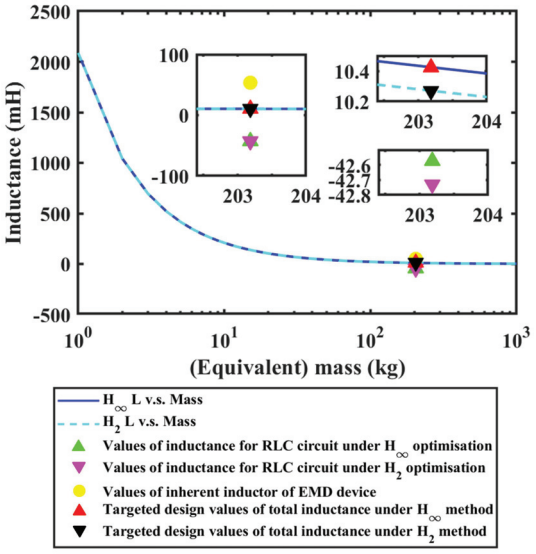

(b) Inductance v.s. equivalent mass

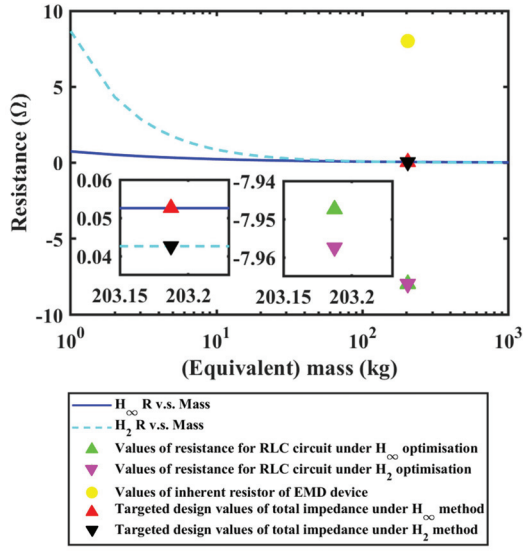

(c) Resistance v.s. equivalent mass

Fig. 12: Relationship between RLC shunt circuit components and equivalent mass under H_∞ and H_2 optimisation design

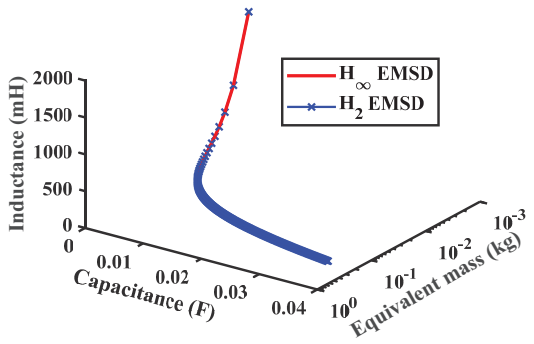

(a) Inductance v.s. capacitance v.s. equivalent mass

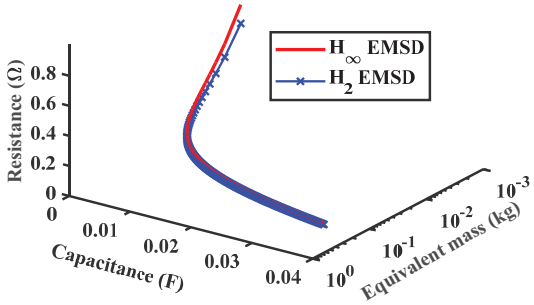

(b) Resistance v.s. capacitance v.s. equivalent mass

Fig. 13: 3D plot of relationship between RLC shunt circuit components and equivalent mass under H_∞ and H_2 optimisation desgin

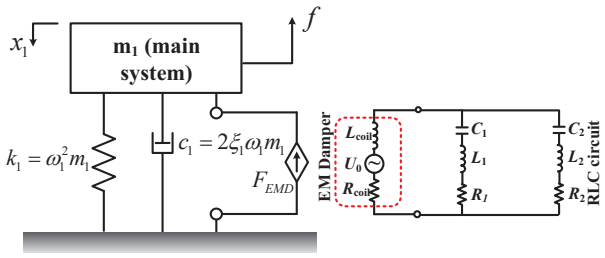

(a) SDOF system with two RLC circuits

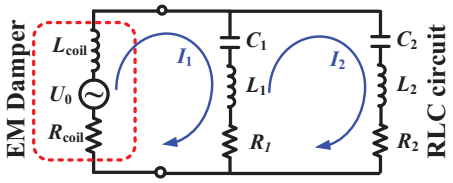

(b) Induced current (eddy current) flowing through the closed EMSD circuit

Fig. 14: SDOF system connected to EMSD (with two RLC circuits)

behaviour via EMSD was proposed in the previous section. However, some studies have selected multi-RC shunt circuits with an EMD to control multiple modes; this mode was proposed by Cheng et al. [28] and Yan et al. [29]. Each shunt circuit is intended to deal with a relevant mode independently. In this section, the proposed H_∞ and H_2 optimal design equations of EMSD (RLC shunt circuit) in the previous section are applied to the test-bed footbridge structure, to demonstrate multi-mode control.

Figure 14a shows the EMSD connected to two RLC resonant shunt circuits. When the vibrational energy activates the EMSD, the machine energy is transferred into electronic energy, based on the electromagnetic coupling effect. This happens in the same way as the process described in the previous section; the difference is that the generating eddy current now flows through two branches of shunt circuits, as shown in Figure 14b.

Using the modal properties of the structure and Equations 21, 22, 33 and 36, the relative FRF curve is presented in Figure 15a. The diagram illustrating the single mode control (TMD) exhibits the classical behaviour that the "with control" peak is divided into two lower magnitude peaks.

In contrast, when looking at the multi-mode control (EMSD), an apparent difference emerges. The TMD control only reduces the magnitude of the second mode a small amount, whereas using EMSD results in a considerable reduction of the second peak. The reason for this effect is that the second frequency of the system is controlled by the optimal design of the second shunt circuit, whereas the TMD is only designed to mitigate single mode dynamics. This demonstrates one of the beneficial results of using an EMSD design. The FRF curves in Figure 15 show that H_2 optimisation still obtains a lower magnitude value than H_∞.

As a result, it appears feasible to mitigate the two modes by connecting two RLC resonant shunt circuits. Therefore, when multi-mode vibration control is to be performed the corresponding number of RLC circuits needs to be connected to the EMD, as illustrated in Figure 16.

The footbridge structure was also used to test multi-mode control of the first five modes using an EMSD. Figure 17 shows the simulation results. In the higher modes, the response was reduced significantly using both H_∞ and H_2 optimisation. However, to control the higher modes simultaneously, control of the first mode might need to be sacrificed.

The H_2 optimisation method considered the control of the wide-bandwidth frequency response. When considering control of both the first and second modes in Figure 15a, the magnitude of the second mode FRF was considerably higher. From this point of view, the second mode had more influence on overall response than the first mode; therefore, the control performance of H_2 was slightly better than H_∞. In contrast, in the first-fifth mode control in Figure 17a, the H_2 method averaged the control effect across a wide frequency bandwidth. Therefore, in this case, H_∞ was more effective than H_2 for control of response in the first mode.

Based on the FRF curves, the single passive TMD is effective only for a single mode, and higher frequency modes exhibit less reduction. The reason for this is that, with its single degree of freedom, a TMD can only effectively control a single mode. To deal with other higher frequency modes,

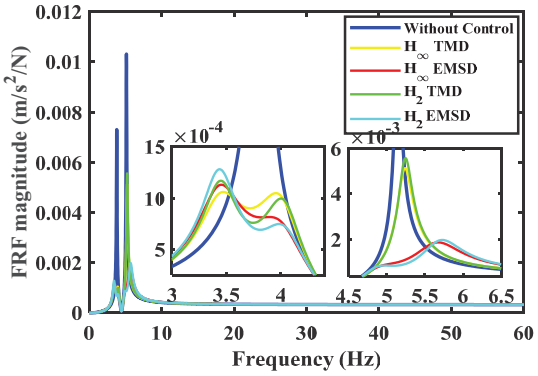

(a) Accelerance FRF magnitude

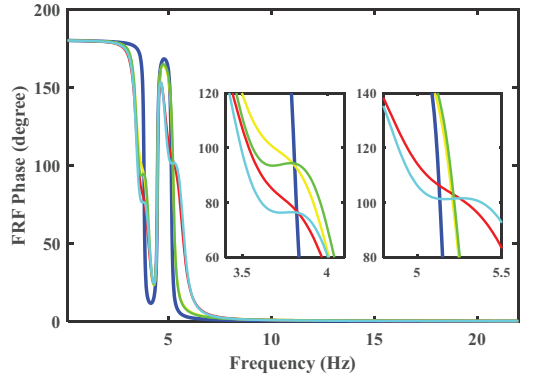

(b) Accelerance FRF phase

Fig. 15: Accelerance frequency response magnitude and phase under H_∞ and H_2 with two RLC resonant shunt circuits

multiple TMDs must be installed, making the design and implementation more complex [37]. However, an EMSD has the potential to control multiple modes, as long as it is connected to an optimally designed shunt circuit with multiple RLC branches, which is relatively straightforward to implement.

5 Discussion and conclusions

The objective of this study has been to examine the potential solution of using EMD devices to provide vibration suppression. An EMD prototype with a shunt circuit consisting of an RLC (resistance-inductance-capacitance) oscillating circuit was utilised to construct EMSD to provide passive shunt damping. H_∞ and H_2 optimisation methods were introduced to obtain the corresponding novel optimal design formulae of the passive EMSD under the random excitation.

The dynamic properties of a laboratory footbridge structure were used for the verification of EMSD vibration mitigation. From the frequency response, the peak magnitude of the FRF curve of the structure was reduced, and the single peak response corresponding with the fundamental mode was split into two lower magnitude peaks. The EMD with RLC resonant shunt circuit exhibited dynamic behaviour equivalent to a TMD. After the optimisation design process, the required resistance and inductance of the device were of high magnitude. Therefore, a negative resistance and inductance circuit was required to scale down the total resistance and inductance.

The equivalent TMD does not involve any moving mass. Theory states that an RLC resonant circuit can act as virtual mass, stiffness, and damping. However, the circuit components respond as a function of the capacitance, which is therefore used to represent the equivalent mass produced in EMSD. The basic concept of TMD suggests that a larger TMD mass ratio can deliver a better control performance, and the analytical study showed similarly that increasing the equivalent mass ratio of the EMSD also produces better controlling results. In the case of real applications, the equivalent mass ratio should take into account the machine capacity and proper magnitude of the nonpolarised capacitance, thus guaranteeing that the device can work within a reasonable range.

Multi-mode control of the system was studied by connecting multiple RLC resonant shunt circuits in parallel. Each parallel RLC circuit's component design was calculated independently in terms of the multiple eigenmodes using the developed H_∞ and H_2 optimisation design schemes. The accelerance FRF showed that using the EMSD with multiple shunt circuits can produce considerable levels of vibration suppression. This type of EMSD multi-shunt circuit design can avoid the arduous implementation issues required for the design of multiple TMDs for control of multiple modes of vibration. Consequently, the developed robust optimal design formulae under the H_∞ and H_2 optimisation could successfully achieve the single and multiple vibration modes suppression. A practical implementation of the EMSD system will be carried out and presented from the author's later publications, to provide an empirical evaluation of this work.

Acknowledgements

The authors would like to acknowledge the financial support provided by UK Engineering and Physical Sciences Research Council (EPSRC) through a Leadership Fellowship Grant (Ref. EP/J004081/2) entitled "Advanced Technologies for Mitigation of Human-Induced Vibration".

References

[1] Efren, D.-j., Rocco, R., Gómez-García, M.-J., and Corral-abad, E., 2019. "Review of Passive Electromagnetic Devices for Vibration". *Shock and vibration,* **2019**(1250707), p. 16.

[2] Yunhe, Y., Nagi G, N., and Rao V, D., 2001. "A literature review of automotive vehicle engine mounting systems". *Shock and vibration,* **36**(1), pp. 123–142.

[3] Nakamoto, E., Chen, Q.-M., Takeuchi, H., and Brauer, J. R., 1997. "Electromagnetic and structural coupled finite element analysis of active control in an anti-vibration device". *IEEE Transactions on magnetics,* **33**(2), pp. 1666–1669.

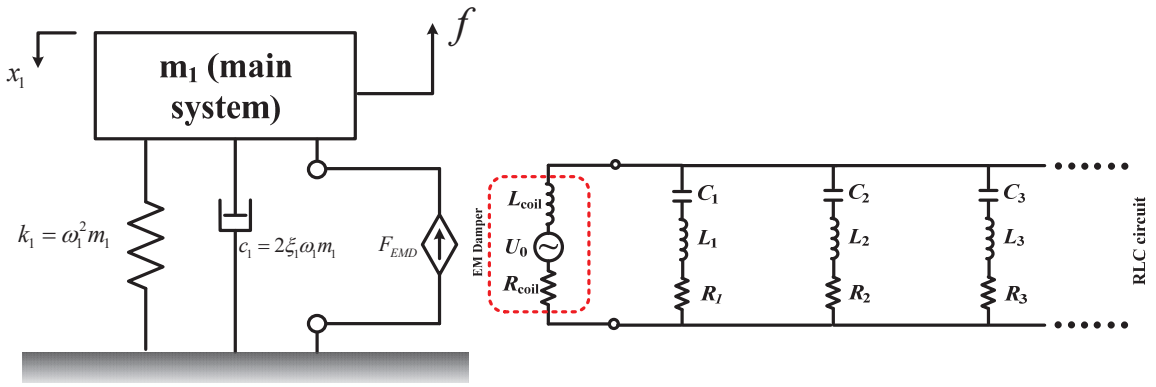

(a) SDOF system with multiple RLC circuits

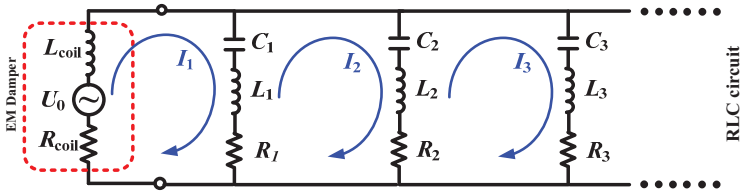

(b) Induced current (eddy current) flowing through the closed EMSD circuit

Fig. 16: SDOF system connected to EMSD (with multiple RLC circuits

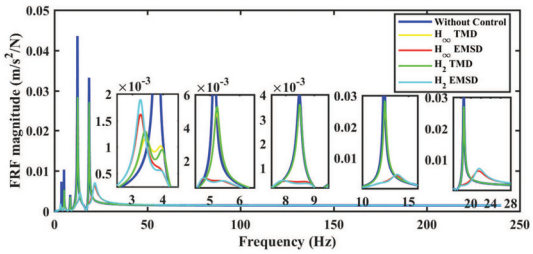

(a) Accelerance FRF magnitude

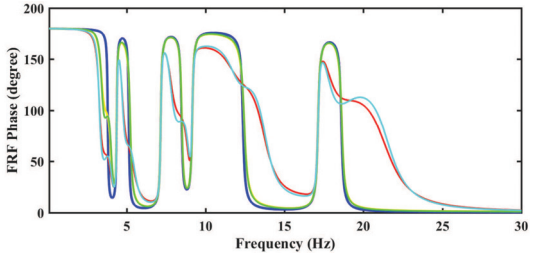

(b) Accelerance FRF phase

Fig. 17: Accelerance frequency response magnitude and phase under H_∞ and H_2 with two RLC resonant shunt circuits

[4] Mizuno, T., Toumiya, T., and Takasaki, M., 2002. "Vibration isolation system using negative stiffness". *JSME International Journal,* **No.02-4224**.

[5] Fleming, A. J., Behrens, S., and Moheimani, S. O. R., 2003. "Active LQR and H2 shunt control of electromagnetic transducers". *42nd IEEE International Conference on Decision and Control (IEEE Cat. No.03CH37475),* **3**, pp. 2294–2299.

[6] Behrens, S., Fleming, A. J., and Reza Moheimani, S., 2003. "Electromagnetic shunt damping". *Proceedings 2003 IEEE/ASME International Conference on Advanced Intelligent Mechatronics (AIM 2003),* **2**(Aim), pp. 1145–1150.

[7] Fleming, A. J., 2004. *Synthesis and implementation of sensor-less shunt controllers for piezoelectric and electromagnetic vibration control*. The University of Newcastle Callaghan PhD Thesis, N.S.W. 2308 Australia.

[8] Behrens, S., Fleming, A. J., and Moheimani, S. O. R., 2005. "Passive vibration control via electromagnetic shunt damping". *IEEE/ASME Transactions On Mechatronics,* **10**(1), pp. 118–122.

[9] Fleming, A. J., and Moheimani, S. O. R., 2006. "Inertial vibration control using a shunted electromagnetic transducer". *IEEE/ASME Transactions On Mechatronics,* **11**(1), pp. 84–92.

[10] Marneffe, B. D., 2007. *Active and passive vibration isolation and damping via shunted transducers*. No. 12. Universite Libre de Bruxelles.

[11] Kim, Y.-B., Hwang, W.-G., Kee, C.-D., and Yi, H.-B., 2001. "Active vibration control of a suspension system using an electromagnetic damper". *Proceedings of the Institution of Mechanical Engineers, Part D: Journal of Automobile Engineering,* **215**(8), pp. 865–873.

[12] Gysen, B. L. J., Paulides, J. J. . H., Janssen, J. L. G., and Lomonova, E. A., 2010. "Active electromagnetic suspension system for improved vehicle dynamics". *IEEE Transactions On Vehicular Technology,* **59**(3), pp. 1156–1163.

[13] van der Sande, T. P. J., Gysen, B. L. J., Besselink, I. J. M., Paulides, J. J. H., Lomonova, E. A., and Nijmeijer, H., 2013. "Robust control of an electromagnetic active suspension system: Simulations and measurements". *Mechatronics,* **23**(2), pp. 204–212.

[14] Palomera-Arias, R., 2005. "Passive electromagnetic damping device for motion control of building structures". Doctor of philosophy in architecture: Building technology.

[15] Palomera-Arias, R., Connor, J. J., and Ochsendorf, J. A., 2008. "Feasibility study of passive electromagnetic damping systems". *Journal of Structural Engineering*(January), pp. 164–170.

[16] Nakamura, Y., Fukukita, A., Tamura, K., Yamazaki, I., Matsuoka, T., Hiramoto, K., and Sunakoda, K., 2013. "Seismic response control using electromagnetic inertial mass dampers". *Earthquake Engineering & Structural Dynamics*, pp. 3–4.

[17] Sodano, H. A., Bae, J.-S., Inman, D. J., and Belvin, W. K., 2006. "Improved concept and model of eddy current damper". *Journal of Vibration and Acoustics*(3), p. 294.

[18] Inoue, T., Ishida, Y., and Sumi, M., 2008. "Vibration suppression using electromagnetic resonant shunt damper". *Journal of Vibration and Acoustics,* **130**(4), p. 041003.

[19] Zhu, S., Shen, W., and Qian, X., 2013. "Dynamic analogy between an electromagnetic shunt damper and a tuned mass damper". *Smart Materials and Structures,* **22**(11), p. 115018.

[20] Cheng, T.-h., and Oh, I.-k., 2009. "Vibration Suppression of Flexible Beam Using Electromagnetic Shunt Damper". *IEEE Transactions on Magnetics,* **45**(6), pp. 2758–2761.

[21] Niu, H., Zhang, X., Xie, S., and Wang, P., 2009. "A new electromagnetic shunt damping treatment and vibration control of beam structures". *Smart Materials and Structures,* **18**(4), p. 045009.

[22] Yan, B., Zhang, X., and Niu, H., 2012. "Vibration isolation of a beam via negative resistance electromagnetic shunt dampers". *Journal of Intelligent Material Systems and Structures,* **23**(6), pp. 665–673.

[23] Yan, B., Zhang, X., Luo, Y., Zhang, Z., Xie, S., and Zhang, Y., 2014. "Negative impedance shunted electromagnetic absorber for broadband absorbing: experimental investigation". *Smart Materials and Structures,* **23**(12), p. 125044.

[24] McDaid, A. J., and Mace, B. R., 2013. "A self-tuning electromagnetic vibration absorber with adaptive shunt electronics". *Smart Materials and Structures*(22), p. 105013.

[25] Zuo, L., and Cui, W., 2013. "Dual-functional energy-harvesting and vibration control: electromagnetic resonant shunt series tuned mass dampers". *Journal of Vibration and Acoustics*(5).

[26] Elliott, S. J., and Zilletti, M., 2014. "Scaling of electromagnetic transducers for shunt damping and energy harvesting". *Journal of Sound and Vibration*, pp. 1–11.

[27] Niederberger, D., Fleming, A., Moheimani, S. O. R., and Morari, M., 2004. "Adaptive multi-mode resonant piezoelectric shunt damping". *Smart Materials and Structures*(5), pp. 1025–1035.

[28] Cheng, T.-H., and Oh, I.-K., 2009. "A current-flowing electromagnetic shunt damper for multi-mode vibration control of cantilever beams". *Smart Materials and Structures,* **18**(9), p. 095036.

[29] Yan, B., Luo, Y., and Zhang, X., 2014. "Structural multimode vibration absorbing with electromagnetic shunt damping". *Journal of Vibration and Control*.

[30] Ao, W. K., and Reynolds, P., 2-5 February, 2015. "Analysis of h_∞ and h_2 optimal design scheme for an electromagnetic damper with shunt resonant circuit". *Proceedings of IMAC-XXXIII Congress, Orlando, FL, USA*.

[31] Ao, W. K., and Chang, K. C., 2010. *Analytical and experimental studies on seismic behavior of structures with building mass dampers*, Vol. 1. National Taiwan University Master of Science Thesis.

[32] Den Hartog, J. P., 1985. *Mechanical vibrations*. Dover Publications Inc., New York.

[33] Cheung, Y., and Wong, W., 2011. "H2 optimization of a non-traditional dynamic vibration absorber for vibration control of structures under random force excitation". *Journal of Sound and Vibration,* **330**(6), pp. 1039–1044.

[34] Wong, W. O., and Cheung, Y. L., 2008. "Optimal design of a damped dynamic vibration absorber for vibration control of structure excited by ground motion". *Engineering Structures*(30), pp. 282–286.

[35] Gradshteyn, I. S., and Ryzhik, I. M., 2007. *Table of integrals, series, and products*, seventh ed ed. The United States of America: Academic Press.

[36] Ao, W. K., 2018. *Electromagnetic damping for control of vibrations in civil structures*. The University of Exeter PhD Thesis, Exeter, Devon, United Kingdom.

[37] Debnath, N., Deb, S., and Dutta, A., 2015. "Multimodal vibration control of truss bridges with tuned mass dampers under general loading". *Journal of Vibration and Control*.